Available online at www.sciencedirect.com
SCIENCE DIRECT
Journal of Catalysis 228 (2004) 347–361
JOURNAL OF CATALYSIS
www.elsevier.com/locate/jcat

Dehydrocondensation of alcohols to form ethers over mesoporous SBA-15 catalyst

Richard G. Herman [a], Fadi H. Khouri [a], Kamil Klier [a,*], John B. Higgins [b], Matthew R. Galler [a], Courtney R. Terenna [a]

[a] *Department of Chemistry, 6 E. Packer Ave., Lehigh University, Bethlehem, PA 18015, USA*
[b] *Air Products and Chemicals, Inc., 7201 Hamilton Boulevard, Allentown, PA 18195, USA*

Received 14 May 2004; revised 31 August 2004; accepted 8 September 2004

Available online 22 October 2004

Abstract

A propylsulfonic acid-derivatized mesoporous SBA-15 catalyst was examined for activity and selectivity in the dehydrocondensation of methanol and isobutanol to form ethers, principally methyl isobutyl ether (MIBE) and dimethyl ether (DME), and dehydration of isobutanol to olefins, at elevated temperatures and pressures. It was shown that the catalyst maintained activity for >1600 h, and the Brønsted acid sites corresponding to 1 meq/g of catalyst were stable under these reaction conditions until they were deliberately in situ poisoned by addition of pyridine. X-ray photoelectron spectroscopy (XPS) revealed that the pyridine was selectively and strongly adsorbed on the sulfonic acid groups. Kinetic studies demonstrated that MIBE and DME were formed by surface-catalyzed S_N2 reactions that follow Langmuir–Hinshelwood kinetics involving competitive adsorption of the alcohols, while isobutene formation utilizes a vacant Brønsted acid site adjacent to the adsorbed isobutanol molecule. Isobutene formation rate exhibited a distinct maximum as a function of the alcohol pressure. This kinetic behavior is similar to that observed with Nafion-H and other catalysts. Because of the high apparent activation energy of isobutene synthesis compared with the much lower apparent activation energies of the ethers, lower reaction temperatures along with higher reactant pressures favor the formation of ethers over olefins. Theoretical modeling of the reaction pathway located stationary points including the transition states (TS) with barrier energies for all reactions involved, and showed that for ether synthesis one alcohol was adsorbed on a sulfonic acid site (I) via a donor H bond while the second alcohol was adsorbed on a proximal sulfonic acid site (II) via an acceptor H bond. In the intermediate, methyl transfer from the adsorbed methanol to the isobutanol oxygen occurs to form MIBE. At the same time, isobutanol donates its proton to a sulfonic acid group (II) whose oxygen acts as a base, and the methanol OH group accepts a proton from a sulfonic acid group (I) and is split off as water. To balance the surface charge, the original proton on sulfonic acid group (II) is transferred to sulfonic acid group (I), and MIBE is desorbed. The flexibility of the TS involving the concerted movement of all three protons is essential for the connectivity of the TS with the reactants and products and the umbrella inversion of the methyl group during its transfer. The theory has thus not only yielded a picture that is fully consistent with observed isotope flows, sp^3 carbon inversion, and temperature/pressure-dependent selectivity, but also revealed unprecedented detail of the concerted proton transfer and the role of acid–base interactions in this dual-site catalysis.

Keywords: Methanol; Isobutanol; Alcohols; Ethers; SBA-15; Brønsted acid; Reaction pathways; Transition states; Methyl isobutyl ether; Dimethyl ether; Isobutene; Mesoporous silica; Sulfonic acid

1. Introduction

There is considerable interest in efficient conversions of natural gas and coal to high-value chemicals and to high-energy, high-purity liquid fuels. The conversion of natural gas and coal to H_2/CO synthesis gas, with H_2/CO typically in the ranges of 2–3 and 0.45–1.0, respectively, are well-

* Corresponding author. Fax: +1 610 758 6536.
E-mail address: kk04@lehigh.edu (K. Klier).

0021-9517/$ – see front matter
doi:10.1016/j.jcat.2004.09.012

established processes [1–3], as is the conversion of synthesis gas to methanol [3–5]. Methanol can be catalytically converted directly to chemicals [6–9] and to a gasoline consisting of a mixture of isoparaffins/aromatics [6,10]. It has been shown that synthesis gas can be directly converted to a mixture of methanol (MeOH) and higher alcohols over heavy alkali base-promoted Cu-based oxide catalysts, with isobutanol (i-BuOH) being the dominant higher alcohol [11–15].

It was found in this laboratory that Nafion-H resins converted the MeOH/i-BuOH mixture to methyl isobutyl ether (MIBE) by acid-catalyzed dehydrocondensation at low temperatures such as 359–389 K and ambient or moderate pressures [16,17], where the MIBE has a high cetane number of 53 [18]. Organic resins were more active for ether synthesis than the Nafion-H resins, but they were less selective and less thermally stable [12,20]. Alternatively, thermally stable inorganic catalysts such as sulfated zirconia and H-ZSM-5 could be used at high temperatures, e.g., 448 K, to give high yields of isobutene (IB) from the alcohol mixture while forming much smaller amounts of the ethers [21]. Isotopic studies of the alcohol coupling reaction over Nafion-H, Amberlyst-35, and H-ZSM-5 indicated that the reaction proceeded via a surface-catalyzed S_N2 reaction with competition of the alcohols for the surface acid sites [22–24]. Ideally, a high-efficiency catalyst designed for the alcohol dehydration/coupling reactions would possess strong Brønsted acid sites in close proximity to one another on a thermally stable, high-surface-area support with low diffusion resistance to the reactants and products.

One approach taken to synthesize a high-efficiency catalyst was to anchor $[–O_3SOCH_2CH_2OSO_3–]^{2-}$ groups on $Zr(OH)_4$ followed by calcination at 500 °C to remove the μ-CH_2CH_2– ligand bridge, yielding surface-grafted acid groups in close proximity to one another on zirconia [25]. The resultant catalyst had significantly enhanced activity and selectivity in producing MIBE from a MeOH/i-BuOH mixture [26]. However, this catalyst had a surface area of 97 m^2/g and an acid-exchange capacity of 0.70 meq H^+/g [25]. Higher surface area and acid concentration would be desirable for a high-efficiency ether synthesis catalyst, and mesoporous supports may yield an improved catalyst.

A family of mesoporous molecular sieves designated as M41S, with MCM-41 as a member, was reported in 1992 [27,28]. These materials exhibited high surface areas and a hexagonal arrangement of uniform parallel 15–100 Å diameter mesopores that adsorbed large amounts of benzene. More recently, a larger pore mesoporous silica, designated as SBA-15, with structural features similar to MCM-41 was synthesized [29,30]. SBA-15 is a well-ordered hexagonal mesoporous silica structure that is synthesized under acidic reaction conditions using an amphiphilic block copolymer as a structure-directing agent [29,30]. This material has a larger unit cell parameter, a larger uniform pore size, a larger pore volume, and thicker silica walls than MCM-41 synthesized by using conventional low-molecular-weight cationic surfactants [30]. It has been reported that SBA-15 is much more hydrothermally stable than the MCM type of materials [29,31].

Similar to the anchoring of 3-mercaptopropyltrimethoxysilane moieties on MCM and hexagonal mesoporous silicas [32–35], SBA-15 has been surface-derivatized with pendant propylthiol groups that can be subsequently or in situ oxidized by $H_2O_{2(aq)}$ to form propylsulfonic acid groups [31]. By X-ray photoelectron spectroscopy, we have shown that oxidation of the thiol (–SH) groups to sulfonic acid ($–SO_3H$) groups is not always complete and can be quantitatively analyzed from photoemissions of the two species [36,37]. The $–SO_3H$ Brønsted acid groups on SBA-15 can be utilized for acid-catalyzed synthesis reactions in gas phase, i.e., coupling of alcohols to form ethers [36], or liquid phase, i.e., esterification of fatty acids with methanol to form methyl esters [38] and synthesis of 2-ethoxytetrahydropyran from 3,4-dihydro-2*H*-pyran and ethanol [33].

In the present research, we investigate the catalytic properties and stability of a large-pore SBA-15 catalyst, prepared in this laboratory and characterized by X-ray powder diffraction (XRD), X-ray photoelectron spectroscopy (XPS), BET surface area, and sorption of nitrogen bases [37], for the dehydrocondensation/dehydration of mixtures of alcohols to form ethers and olefins and probe the mechanistic pathway and reaction intermediates involved in these reactions. The advantages of large-pore silica-based materials are in applicability to reactions of large molecules and nonswelling properties.

2. Experimental procedures

2.1. Catalyst synthesis

The SBA-15 catalyst was synthesized at 313 K from tetraethoxysilane (TEOS, Aldrich) and 3-mercaptopropyltrimethoxysilane (MPTMS, Aldrich) with Pluronic 123 $EO_{20}PO_{70}EO_{20}$ triblock copolymer (MW = 5800, Aldrich) as the templating agent using the one-step direct synthesis procedure of Margolese et al. [31] and as described previously [37]. Following prehydrolysis of TEOS and Pluronic 123, MPTMS and H_2O_2 (30%, Aldrich) were added and the mixture was equilibrated for 20 h. After further aging at 373 K for 24 h, the white precipitate was filtered, air-dried at ambient temperature, and then refluxed in 95% ethanol for 24 h (200 ml of ethanol/1.5 g of dried solid) to extract any remaining Pluronic template. The material was then filtered, washed sequentially with distilled water and absolute ethanol, and dried in an oven at 333 K.

2.2. Determination of activity and selectivity

The activity and selectivity of the SBA-15 catalyst was determined for the dehydration and coupling of alcohols us-

ing methanol/isobutanol (MeOH/i-BuOH) = 1/1 and 2/1 molar ratio mixtures fed into nitrogen carrier gas using an ISCO high-pressure pump. The catalyst (0.40 g) was diluted with 8 ml 3 mm Pyrex beads, and the bed was held in place in the reactor with additional beads below and above the bed. The reactor consisted of a downflow 0.75-inch o.d. (0.120-inch wall thickness) 316 stainless-steel reactor containing an axial thermocouple well for monitoring the catalyst temperature. The catalyst was first purged with a flow of N_2 at ambient pressure (1 atm = 0 psig = 101.3 kPa) that was monitored and controlled by a Porter mass-flow meter. After heating the catalyst bed to above 373 K, the alcohol mixture was injected into the N_2 stream at the top of the reactor in a preheated mixing zone before entering the vertical reactor contained in a three-zone furnace. For testing with MeOH/i-BuOH = 1/1, the reactant flow was MeOH/i-BuOH/N_2 = 1.72/1.72/16 mol/(kg_{cat} h) with gas hourly space velocity (GHSV) ≈ 475 L/(kg_{cat} h), and the temperature sequence utilized was 382, 388, 394, 398, 403, 408, 391, 385, 379, and 375 K. For testing with MeOH/i-BuOH = 2/1, the reactant flow was MeOH/i-BuOH/N_2 = 10.4/5.2/184 mol/(kg_{cat} h) with GHSV ≈ 4870 L/(kg_{cat} h), and the temperature dependence was determined in the sequence 389, 393, 399, 404, 409, 414, 418, 406, 396, 386, and 401 K. The reactor pressure in the range of 0.1–4.6 MPa was controlled by an in-line Mity-Mite back-pressure regulator located between the reactor and the gas chromatograph. The back-pressure regulator and all exit lines were heated to 423–443 K.

Analysis of the reactants and products was carried out by gas chromatography (GC) using a CP-SIL 5CB WCOT dimethylpolysiloxane column (30 m × 0.25 mm i.d.) in a Hewlett–Packard (HP) Model 5890 Series II GC. The GC was coupled with a HP Model 3396 Series II integrator/controller unit that was interfaced with an automated heated, in-line Valco sampling valve. The thermal response factors (TRFs) of the analyzed compounds were calibrated, and the following values were used: nitrogen (42), water (33), methanol (MeOH, 50), isobutanol (i-BuOH, 125), dimethyl ether (DME, 75), methyl isobutyl ether (MIBE, 125), methyl tertiarybutyl ether (MTBE, 125) isobutene (IB, 93), *n*-butenes (97), diisobutyl ether (DIBE, 220), and tertiarybutylisobutyl ether (TBIBE, 220). Data points presented here are generally averages of 3–10 GC analyses obtained under steady-state conditions that were usually maintained for 6–24 h.

2.3. Kinetic modeling

Kinetic analyses of the data were carried out based on Langmuir–Hinshelwood competitive adsorption of the alcohols on the reactive acid centers of the catalyst. As pointed out earlier [22–24], this is a simplified approach that nevertheless successfully describes the competitive nature of the reactions occurring on the catalyst surface. This kinetic treatment was described previously [17], and the rate laws used here for the formation of the products are the following:

$$r_{\mathrm{DME}} = k_1 K_{\mathrm{M}}^2 p_{\mathrm{M}}^2/(1 + K_{\mathrm{M}} p_{\mathrm{M}} + K_{\mathrm{B}} p_{\mathrm{B}})^2, \quad (1)$$

$$r_{\mathrm{IB}} = k_3 K_{\mathrm{B}} p_{\mathrm{B}}/(1 + K_{\mathrm{M}} p_{\mathrm{M}} + K_{\mathrm{B}} p_{\mathrm{B}})^2, \quad (2)$$

$$r_{\mathrm{MIBE}} = k_4 K_{\mathrm{M}} p_{\mathrm{M}} K_{\mathrm{B}} p_{\mathrm{B}}/(1 + K_{\mathrm{M}} p_{\mathrm{M}} + K_{\mathrm{B}} p_{\mathrm{B}})^2. \quad (3)$$

In these expressions, k_1, k_3, and k_4 are the kinetic rate constants for DME, IB, and MIBE synthesis via Eqs. (4)–(6), respectively, and K_{M} and K_{B} are the adsorption equilibrium constants for methanol and isobutanol, respectively, while p_{M} and p_{B} are the partial pressures of alcohol reactants

$$2CH_3OH \rightarrow CH_3OCH_3 + H_2O, \quad (4)$$

$$(CH_3)_2CHCH_2OH \rightarrow (CH_3)_2C{=}CH_2 + H_2O, \quad (5)$$

$$(CH_3)_2CHCH_2OH + CH_3OH \rightarrow (CH_3)_2CHCH_2OCH_3 + H_2O. \quad (6)$$

2.4. Surface analysis

High-resolution X-ray photoelectron spectroscopy analysis was carried out using the Scienta ESCA-300 instrument, as described in detail elsewhere [37]. Based on estimates by Hunsicker et al. [39], XPS analysis of very porous materials provides a bulk analysis because of the large escape depths. All binding energy (BE) values reported herein are referenced to the Si2p BE of 103.5 eV.

The BET surface area [40] was determined by N_2 adsorption at 77 K in the relative pressure range (P/P_o) of 0.05 to 0.30 using a Micromeritics Gemini 2360 V1.03 instrument. An adsorption isotherm was also obtained, and the total pore volume was estimated from the amount of N_2 adsorbed at $P/P_o = 0.975$. Before the measurements, the SBA-15 sample was purged in flowing N_2 in the sample tube at 473 K for 2 h. The mesopore size distribution was calculated on the basis of the adsorption branch of the N_2 isotherm using the Barrett, Joyner, and Halenda (BJH) method [29,30,41–45].

To determine the accessible acidity of the catalyst (meq/g), a 50-mg portion, after drying at 200 °C in flowing N_2 for 1 h, was equilibrated in 15 ml 2.0 M $NaCl_{(aq)}$ at ambient temperature. Phenolphthalein was then added, and the titration of the mixture with 0.01 M $NaOH_{(aq)}$ was also followed potentiometrically.

2.5. Electron microscopy and X-ray powder diffraction

Bright-field transmission electron microscopy (TEM) images were obtained on a JEOL 2000FX microscope at the Center for Advanced Materials and Nanotechnology at Lehigh University. Samples were prepared by dispersing a small amount of SBA powder in 10 ml of ethanol and sonicating the dispersion in an ultrasonic bath. A drop of the dispersion was placed on a holey carbon grid for examination in the TEM at 200 kV after evaporation of the ethanol. X-Ray powder diffraction was used to monitor crystallinity and interlayer spacings for the hexagonal SBA-15 using the low-angle 2θ peaks. The XRD data were collected on

a Siemens D5000 instrument with Cu$K\alpha$ radiation as described previously [37].

2.6. Computational modeling and analysis

The sulfonic acid-catalyzed reactions of ethers from alcohols were first examined theoretically via DFT/GGA/DN** calculations based on the Nafion-type prototype system $2CF_3SO_3H + CH_3OH + (CH_3)_2CHCH_2OH$ [46]. This investigation has now been extended to the much larger model of mesoporous silica derivatized with pendant propylsulfonic acid functionalities. The model for the dual site consisted of two propylsulfonic groups anchored on two silicon atoms capped by two hydrogen each and bridged by oxygen, of the composition $HO_3S(CH_2)_3$–$Si(H_2)$–O–$Si(H_2)$–$(CH_2)_3SO_3H$, abbreviated as $G{=}(OH)_2$. The structural unit –[$Si(H_2)$–O–$Si(H_2)$]– was taken to represent the silica intraporous wall. The reaction models comprised adducts:

(**I**) $[G{=}(OH)_2][2MeOH]$,
(**II**) $[G{=}(OH)_2][MeOMe][H_2O]$,
(**III**) $[G{=}(OH)_2][MeOH][i\text{-}BuOH]$,
(**IV**) $[G{=}(OH)_2][i\text{-}BuOMe][H_2O]$,
(**V**) $[G{=}(OH)_2][i\text{-}BuOH]$, and
(**VI**) $[G{=}(OH)_2][i\text{-}Bu^{=}][H_2O]$.

Reaction pathways (**I**) → (**II**), (**III**) → (**IV**), and (**V**) → (**VI**) represent the synthesis of DME, MIBE, and dehydration of i-BuOH to isobutene i-Bu$^{=}$. The transition states (TS) on these three pathways were searched and located, in addition to pre- and postreaction surface complexes.

The present calculations employed all-electron codes imbedded in the Titan software using the DFT = Slater + Becke88 + PZ81 + Perdew86 method with the 6-31G** basis set [47]. The 6-31G** Gaussian basis set gave comparable *relative* energies to the earlier used double numerical basis set DN** [46], although the *absolute* energies were systematically higher with the 6-31G** set than with the DN** set. Geometry optimization for each of the adducts (**I**)–(**VI**) involved a "frozen wall" unit –[$Si(H_2)$–O–$Si(H_2)$]– and allowed all other atoms of these complexes to move to their equilibrium positions. The TS search looked for stationary saddle points on the paths (**I**) → (**II**), (**III**) → (**IV**), and (**V**) → (**VI**) and involved vibrational frequency analysis, including the calculation of the imaginary mode associated with saddle-point crossings and group transfers from one adsorbed reactant to another. Such saddle points and imaginary frequencies were found for all three pathways. Those for the DME synthesis, (**I**) → (**II**), and the MIBE synthesis, (**III**) → (**IV**), were determined more easily, primarily due to successful TS calculations on earlier smaller models [46]. However, the search for the TS for the seemingly simpler dehydration of i-BuOH to i-Bu$^{=}$ and H_2O, (**V**) → (**VI**) has proven extraordinarily difficult, involving many initial guesses of the adsorbed conformations and many month-long computations on 2GHz/2GB machines, but eventually was successful in locating the TS and unraveling a new indirect path for this dual-site-catalyzed elimination reaction.

3. Results

3.1. TEM and XRD of the SBA-15 material

Micrographs showed the long-range order of the SBA-15 catalyst, as shown in Fig. 1. The pore center-to-pore center dimension of the mesopores measured from micrographs of multiple particles was approximately 11 nm. Low-angle

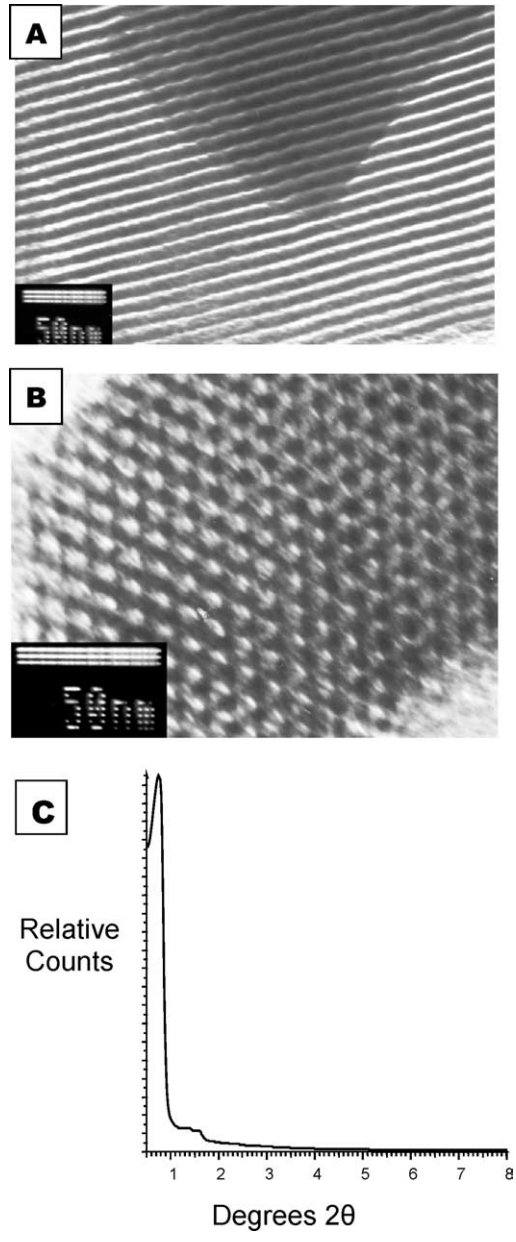

Fig. 1. Transmission electron micrographs of the as-synthesized SBA-15 catalyst showing (A) the view perpendicular to the pore axes, (B) the close-packed hexagonal structure of parallel pores shown from the sixfold symmetry axis of view, and (C) the small-angle XRD pattern.

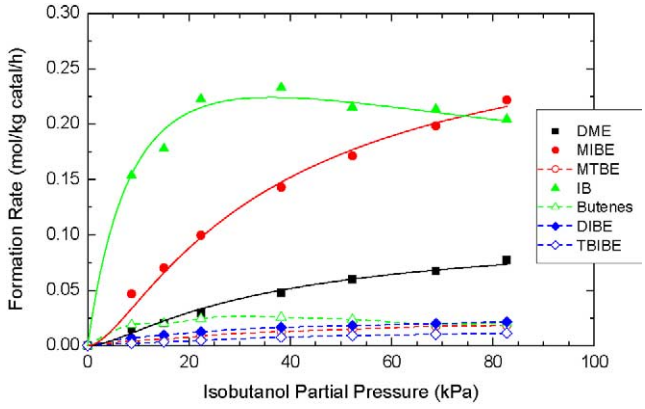

Fig. 2. Rates of formation of dimethyl ether (DME), isobutene (IB), methyl isobutyl ether (MIBE), diisobutyl ether (DIBE), *n*-butenes (*cis*- and *trans*-2-butenes), methyl tertiary butyl ether (MTBE), and tertiary butyl isobutyl ether (TBIBE) in the reaction of MeOH/i-BuOH (1/1 molar ratio) over the SBA-15 catalyst with flow rates of 3.44 mol/(kg_{cat} h) alcohols and 16.0 mol/(kg_{cat} h) of N_2 at 404 K as a function of isobutanol partial pressure, $p_{i\text{-BuOH}}$, are given as data points. The fitted kinetic laws [Eqs. (1)–(3), with the values of the kinetic parameters given in Section 4.1.1. under Discussion] for IB, MIBE, and DME syntheses are shown as solid curves for those three products.

XRD of the material yielded the expected diffraction pattern [31] shown in Fig. 1C with $d_{100} \approx 12$ nm.

3.2. Methanol/isobutanol reactions

3.2.1. Pressure dependence with MeOH/i-BuOH = 1/1

After establishing N_2 flow through the reactor at 101.3 kPa (0 psig) total pressure, the SBA-15 catalyst was heated to 404 K. Injection of the alcohol mixture was initiated so that the steady reactant flow rates were 3.44 mol/(kg_{cat} h) of alcohols and 16.0 mol/(kg_{cat} h) of carrier gas, giving a total gas hourly space velocity (GHSV) of about 475 l (STP)/(kg_{cat} h). After equilibration for 21 h, the reactor pressure was sequentially increased. The observed product formation rates are shown in Fig. 2. In addition to IB, MIBE, and DME, methyl tertiary butyl ether (MTBE), *cis*- and *trans*-2-butenes, diisobutyl ether (DIBE), and tertiary butyl isobutyl ether (TBIBE) were also observed as minor products. IB exhibited the highest selectivity at low pressures. As the pressure was increased, the formation and selectivity toward MIBE steadily increased, while the selectivity to DME increased more gradually and that to IB decreased.

3.2.2. Temperature dependence with MeOH/i-BuOH = 1/1

The reactor was purged with an N_2 flow at 101.3 kPa and about 380 K, and then alcohol injection was initiated. The temperature dependence of the reactions involved was carried out as described in Section 2.2.

Arrhenius plots were used to determine the apparent activation energies of the products formed at 101.3 kPa. As shown in Fig. 3, the plots were linear in the temperature range of 375–408 K that was employed here. In this temperature range, the conversions of methanol and isobutanol varied from 0.73 to 9.23% and from 0.91 to 23.30%, respectively. Due to higher activation energy, IB became a dominant product at >383 K.

3.2.3. Pressure dependence with MeOH/i-BuOH = 2/1

This reactant composition was investigated because it favors ether formation, and a higher flow rate was utilized for comparison with previous studies with other acid cat-

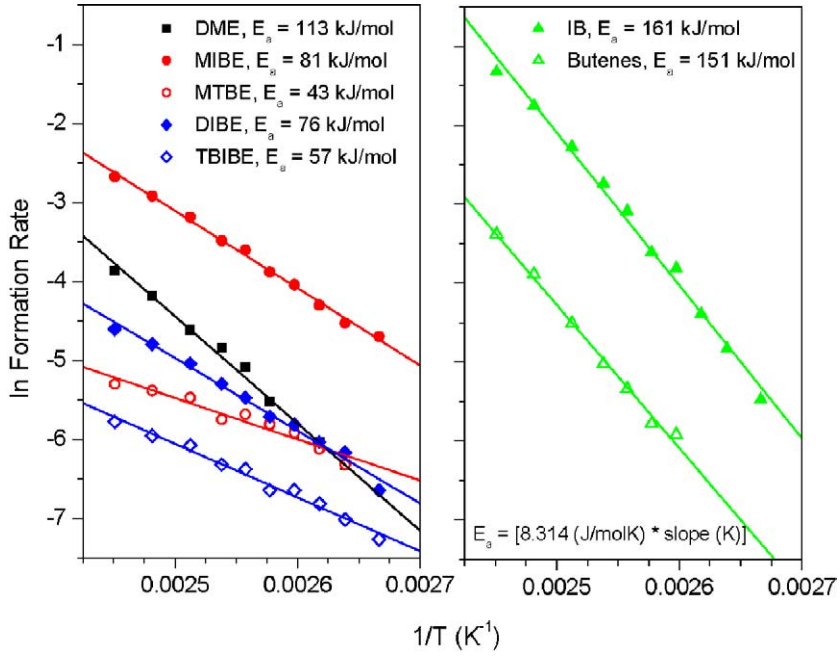

Fig. 3. Arrhenius plots for determination of the apparent activation energies of the ethers (right) and olefins (left) formed over the SBA-15 catalyst from the MeOH/i-BuOH = 1/1 reactant mixture at 101.3 kPa.

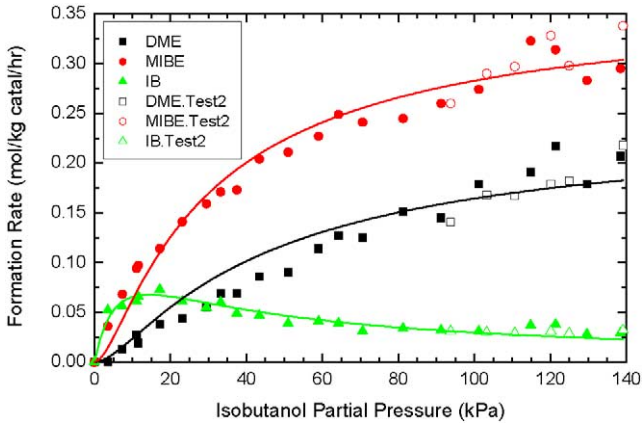

Fig. 4. Rates of formation of DME, IB, and MIBE in the reaction of MeOH/i-BuOH (2/1 molar ratio) over the SBA-15 catalyst with flow rates of 16.5 mol/(kg_{cat} h) alcohols and 184 mol/(kg_{cat} h) of N_2 at 404 K as a function of isobutanol partial pressure, $p_{i\text{-BuOH}}$, are given as data points. The open symbols represent a second test sequence of the catalyst after the first test (closed symbols) was completed and the catalyst was purged with nitrogen at ambient pressure before repressurizing to the higher range of pressures. The fitted kinetic laws [Eqs. (1)–(3), with the kinetics parameters given in Section 4.1.2. under Discussion] are shown as solid curves.

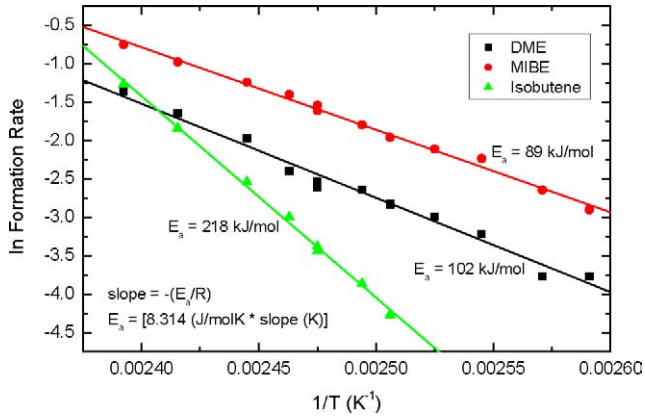

Fig. 5. Arrhenius plots for the determination of the apparent activation energies of the products formed over the SBA-15 catalyst from the MeOH/i-BuOH = 2/1 reactant mixture at 2.17 MPa.

alysts [16,17,26,36]. After heating the SBA-15 catalyst to 404 K in flowing N_2 at 115 kPa (2 psig) total pressure, injection of the alcohol mixture was initiated and the reactant flow rates were adjusted to MeOH/i-BuOH/N_2 = 12.3/6.2/184 mol/(kg_{cat} h), corresponding to GHSV = 4950 L/(kg_{cat} h). The total reactor pressure was then increased sequentially to 4.525 MPa (642 psig), during which the partial pressures of both alcohols increased proportionally. The rates of formation of the DME, IB, and MIBE products are shown in Fig. 4. The solid curves were obtained by fitting the data points using kinetic Eqs. (1)–(3) of Section 2.3.

3.2.4. Temperature dependence with MeOH/i-BuOH = 2/1

The reactor pressure was adjusted to 2.17 MPa and the temperature was initially set at 404 K. Injection of the alcohol reactant mixture was initiated, and the temperature dependence of the catalytic behavior of the SBA-15 catalyst was determined. The formation rates of MIBE, DME, and IB increased with temperature, and MIBE remained the dominant product formed over the temperature range utilized. Only traces of MTBE, DIBE, and TBIBE were observed at this flow rate that was appreciably higher than that utilized for the MeOH/i-BuOH = 1/1 experiments. The DME selectivity decreased slightly with increasing temperature, while the MIBE selectivity decreased more significantly as that of IB increased. The Arrhenius plots of the rate data, given in Fig. 5, showed that the apparent activation energy for isobutanol dehydration to form isobutene was more than twice as high as for the synthesis of the ethers under these reaction conditions.

Table 1
Formation rates of products (mol/(kg_{cat} h)) as a function of time on stream at 404 K and 2.17 MPa with MeOH/i-BuOH/N_2 = 10.4/5.2/184 mol/(kg_{cat} h)

Time on stream (h)	MIBE	DME	IB
(a) 11.5–13.5	0.200	0.078	0.030
(b) 66.25–68.25	0.200	0.079	0.034
(c) 115.25–116.5	0.214	0.074	0.032

3.3. Catalyst stability

During the determination of catalytic properties with alcohol mixtures, the catalyst was subjected to elevated temperature and pressure conditions for 1615 h. In addition, it was purged with N_2 alone at elevated temperatures and at either ambient pressure (297 h) or elevated pressure (291 h) between experiments and when the alcohol mixture in the ISCO injection pump was being changed. With a reactant mixture of MeOH/i-BuOH/N_2 = 10.4/5.2/184 mol/(kg_{cat} h) at 404 K, the reaction pressure was increased to 2.17 MPa and the reaction was allowed to run at steady state overnight. The results are shown in Table 1. After determining the activity of the catalyst under these conditions (as shown in row (a), Table 1), pressure dependence experiments were conducted at sequentially increasing pressures to 4.39 MPa. The pressure was then reduced to 2.17 MPa to again determine the steady-state activity under the initial conditions (row (b), Table 1). Continuous operation of the reactor was maintained for an additional 48 h, and the results are shown in row (c), Table 1. Each of the product formation rates is an average of five to six analyses.

3.4. Site blocking by pyridine

Our previous studies have utilized pyridine as a probe to determine the nature, strength, and concentration of acid sites on surfaces of solid catalysts [25,37,46,48]. In particular, quantitative XPS data provide this information following

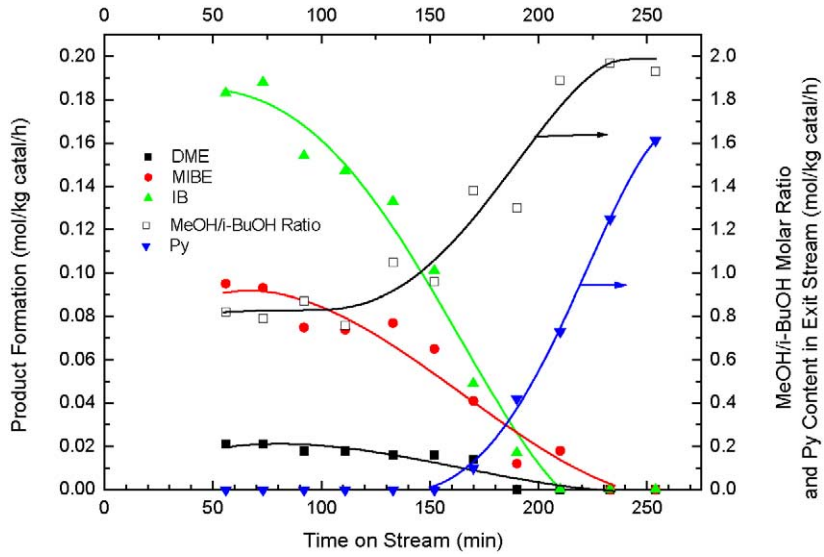

Fig. 6. Deactivation of the SBA-15 catalyst at 404 K and 375 kPa upon changing the reactant gas mixture from MeOH/i-BuOH/N_2 = 7.4/7.4/184 mol/(kg_{cat} h) to MeOH/i-BuOH/Py/N_2 = 10.4/5.2/1.04/183 mol/(kg_{cat} h) with GHSV = 4870 L/(kg_{cat} h).

adsorption of nitrogen bases on the acid sites. To determine whether pyridine in the reactant alcohol mixture retarded the synthesis of ethers by adsorption and site blocking, pyridine was added to the reactant stream. After purging the catalyst with N_2 at 400 K and 375 kPa, reactant alcohol injection was initiated, briefly with a MeOH/i-BuOH = 1/1 mixture that was followed by a mixture of MeOH/i-BuOH/Py = 2/1/0.2. Fig. 6 shows the resulting product formation rates, MeOH/i-BuOH molar ratio, and appearance of pyridine in the outlet stream, as determined by GC analyses as a function of time on stream.

After the pyridine poisoning experiment, reactant injection was terminated and the reactor was purged with N_2 at 403 K and 375 kPa for 65 h. Injection of a MeOH/i-BuOH/N_2 = 10.4/5.2/184 mol/(kg_{cat} h) reactant flow was then started. The inlet line between the pump and the N_2 carrier gas line in the preheater section above the reactor contained some remaining MeOH/i-BuOH/Py reactant mixture, but most of the pyridine had been purged from the system within 3 h on stream. However, there was still a trace of pyridine present in the chromatograms after 24 h, and there was no evidence of products formed from the MeOH/i-BuOH reactant mixture. The reaction temperature was increased to 423 K, and a small amount of MIBE was formed, amounting to 0.02–0.03 mol/(kg_{cat} h) over the next 24 h. No DME and IB formation was observed. The temperature was then increased to 473 K, and after 3 h the steady-state formation rates for MIBE, DME, and IB were approximately 0.220, 0.070, and 0.020 mol/(kg_{cat} h), respectively. The temperature was decreased to 423 K, and after 15 h the steady-state synthesis rate of MIBE was 0.02–0.03 mol/(kg_{cat} h). Again, no DME and IB were observed. Comparison of the activities of the catalyst at similar pressures before and after pyridine exposure is shown in Table 2. Alcohol coupling was still observed at the higher temperature and pressure after pyridine adsorption, but the initial activity was not fully recovered.

Table 2
Comparison of the space time yields (mol/(kg_{cat} h)) of the products before and after pyridine (Py) addition to the reactant stream consisting of MeOH/i-BuOH/N_2 = 10.4/5.2/183–184 mol/(kg_{cat} h)

Total pressure (kPa)	Temperature (K)	MIBE	DME	IB
Before Py addition				
365	404	0.069	0.017	0.052
1140	404	0.135	0.042	0.042
After Py addition				
375	403	–	–	–
	423	0.02–0.03	–	–
	473	0.220	0.070	0.020
1080	403	0.016	–	–
	423	0.044	0.008	–

The entry (–) indicates not detected.

The alcohol injection was terminated and the reactor was purged with N_2 at 403 K for 23 h, first at 375 kPa and then at 108 kPa. Injection of the MeOH/i-BuOH = 2/1 reactant was begun again at 403 K and 108 kPa, and the reactor pressure was gradually increased from 108 to 1080 kPa over a period of 46 h. No products were observed at the lower pressures, but at 1080 kPa the sole product MIBE was observed (0.016 mol/(kg_{cat} h)). At this latter pressure, the temperature was increased to 423 K and steady state was maintained for 43 h. Under these conditions, the formation rates of MIBE and DME were 0.044 and 0.008 mol/(kg_{cat} h), respectively, and no IB was observed (see Table 2). After terminating alcohol injection, the reactor was depressurized and cooled slowly while purging the catalyst with N_2 over a period of 27 h. The catalyst was then removed from the reactor under an N_2 environment for examination by other methods. The tested catalyst was an off-white light gray color compared with the white as-prepared catalyst.

3.5. Properties of the tested catalyst

The tested and partially deactivated catalyst was analyzed by XPS. Both the survey and higher resolution C1s, S2p, N1s, O1s, and Si2p binding energy (BE) spectra were obtained. The O1s and Si2p BE peaks were symmetrical, and the O1s peak was centered at 532.75 eV. The C1s spectrum showed a strong peak at 285.2 eV, with a higher BE shoulder that was resolved as a broad peak centered at 286.6 eV. The observed $C/S_{(Total)}$ ratio of 10.7 indicated excess carbon deposited on the used off-white gray catalyst. The S2p peak was broad and the $S2p_{1/2}$ and $S2p_{3/2}$ spin–orbit splitting was not evident in the spectrum, as noted in previous studies with SBA-15 [36,37]. The S2p peak asymmetry was fitted as two peaks with BEs of S(1) = 169.1 and S(2) = 167.8 eV, with relative intensities corresponding to 72 and 28% of the total sulfur, respectively. These BEs indicate that both S species were present in a highly oxidized state [52]. An N1s peak was centered at 402.2 eV with a slight tail to lower BEs. This peak position is consistent with a hydrogen-bonded pyridinium-type species but not with nitrate [37,48–50] since the latter species is typically observed at higher binding energies of 407.6 ± 0.5 eV. The overall $N/S_{(Total)}$ ratio was calculated from the XPS spectra to be 0.28 ± 0.02. After outgassing at 473 K, the BET surface area of the tested, partially poisoned SBA-15 catalyst was 314 m^2/g.

3.6. Quantum mechanical modeling of the reaction pathways for the principal reactions: (I) → (II) for DME, (III) → (IV) for MIBE, and (V) → (VI) for dehydration of i-BuOH to IB

In this effort we employed *all-electron* computational analysis for calculations of the following properties: structures and total energies (a) of the reactants in the prereaction adsorbed complex, (b) of the products in the postreaction adsorbed complex, (c) of the transition states at the saddle points; vibrational frequencies focusing on the imaginary mode and motion in the TS, and orbital energies including the core levels that were previously shown to account for the XPS binding energy shifts were observed in both the sorption sites and adsorbates upon the surface complex formation [37]. All the structures were optimized with the –[Si(H_2)–O–Si(H_2)]– "wall" frozen, as described in Section 2.6. The calculated total energies are summarized in Table 3.

Here the difference between energies of the adsorbed products and reactants represents the thermodynamic driving force for the surface reaction, and the difference between energy of the TS and the reactants is the barrier on the potential energy surface for each of the processes (**I**) → (**II**) for DME, (**III**) → (**IV**) for MIBE, and (**V**) → (**VI**) for IB. Table 4 summarizes the imaginary vibrational frequencies found for each TS. Of these, the largest imaginary frequencies are associated with motions along the reaction pathway, i.e., of methyl group from MeOH to the second alcohol in the formation of ethers, and of the hydrogen of C-2 of i-BuOH to the surface sulfonic group. These "reaction modes" are boldfaced in Table 4. The smaller imaginary frequencies involve mainly torsional oscillations of the "wall" unit and are irrelevant to the reaction path.

The paths for DME and MIBE are very similar, and are exemplified in Fig. 7 by the process (**I**) → (**II**) for DME. The initial adsorption of DME on the sulfonic acid sites results in the formation of the G=$(OH)_2(MeOH)_2$ complex, as shown in Fig. 7, left, where distances are shown in Å.

Table 3
Total energies of sorption complexes of reactants, products, and transition states for the dual-site catalyzed dehydrocondensation of methanol with MeOH to DME, of MeOH with i-BuOH to MIBE, and dehydration of i-BuOH to IB (the models, calculation method, and optimization protocol are given in Section 2.6)

Complex[a]	Energy (Hartree)	ΔE (kJ/mol)[b]
G=$(OH)_2(MeOH)_2$	−2372.97484	
G=$(OH)_2$(DME)(H_2O)	−2472.97577	−2.4[c]
G=$(OH)_2$(MeOH)(i-BuOH)	−2490.92086	
G=$(OH)_2$(MIBE)(H_2O)	−2490.92010	+2.0[d]
G=$(OH)_2$(i-BuOH)	−2375.19690	
G=$(OH)_2$(i-Bu$^=$)(H_2O)	−2375.18073	+42.4[e]
TS-DME	−2372.94713	+72.7[c]
TS-MIBE	−2490.88920	+83.1[d]
TS-IB	−2375.14019	+148.8[e]

[a] G=$(OH)_2$ is the dual-site $HO_3S(CH_2)_3$–Si(H_2)–O–Si(H_2)–$(CH_2)_3SO_3H$; TS-DME, TS-MIBE and TS–IB are transition states for DME, MIBE, and IB formation on the dual-site G=$(OH)_2$.
[b] Energy difference of the products from the sorbed reactant complex.
[c] G=$(OH)_2(MeOH)_2$.
[d] G=$(OH)_2$(MeOH)(i-BuOH).
[e] G=$(OH)_2$(i-BuOH).

Table 4
Imaginary vibrational frequencies at the transition states for the formation of dimethyl ether (DME), methyl isobutyl ether (MIBE), and dehydration isobutene (IB) (the models, calculation method and optimization protocol are given in Section 2.6)

Complex[a]	Imaginary frequencies (cm^{-1})	Character of motion
TS-DME	**394.43**	Methyl group transfer with proton transfer
	86.03	CH_2–(SiH_2)–O– rocking
	65.87	O–(SiH_2)–CH_2 rocking
	13.20	Delocalized mode
TS-MIBE	**394.84**	Methyl group transfer with proton transfer
	92.41	CH_2–(SiH_2)–O– rocking
	64.20	O–(SiH_2)–CH_2 rocking
	30.28	Delocalized mode
	18.27	Delocalized mode
TS-IB	**700.75**	Hydrogen transfer C ↔ H ↔ O=S
	57.38	CH_2–(SiH_2)–O– rocking
	40.31	O–(SiH_2)–CH_2 rocking
	21.54	Delocalized mode
	6.11	Delocalized mode

[a] TS-DME, TS-MIBE, and TS–IB are the transition states for DME, MIBE and IB formation over the dual-site G=$(OH)_2$.

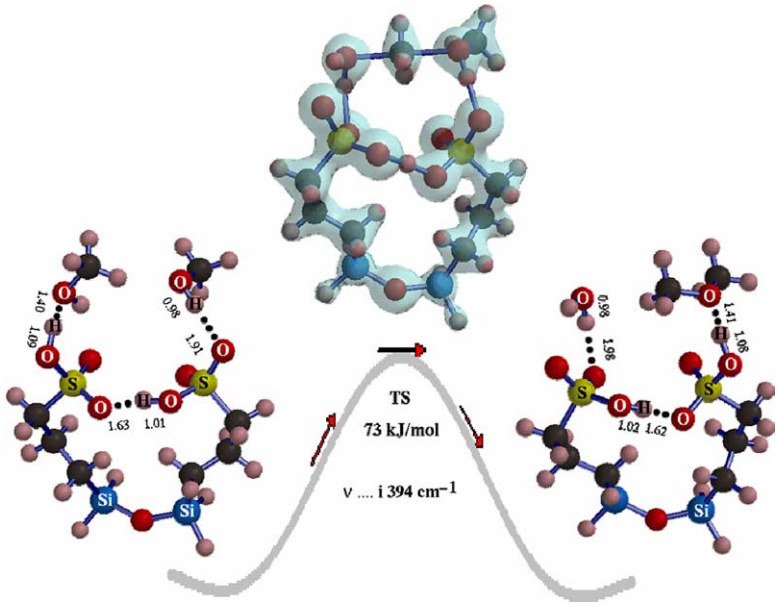

Fig. 7. The optimized configuration (left) for the adsorption of two MeOH molecules on the dual sulfonic acid centers on the SBA-15 catalyst. The transition state for DME synthesis over SBA-15 is shown in the middle of the figure, where electron density is shown as a transparent isosurface to within 0.08 electrons/a.u.^{3} The optimized configuration of adsorbed DME and H_2O product molecules on the dual sulfonic acid centers of the SBA-15 catalyst is shown on the right. Selected distances of importance to the adsorption and reaction are given in Å.

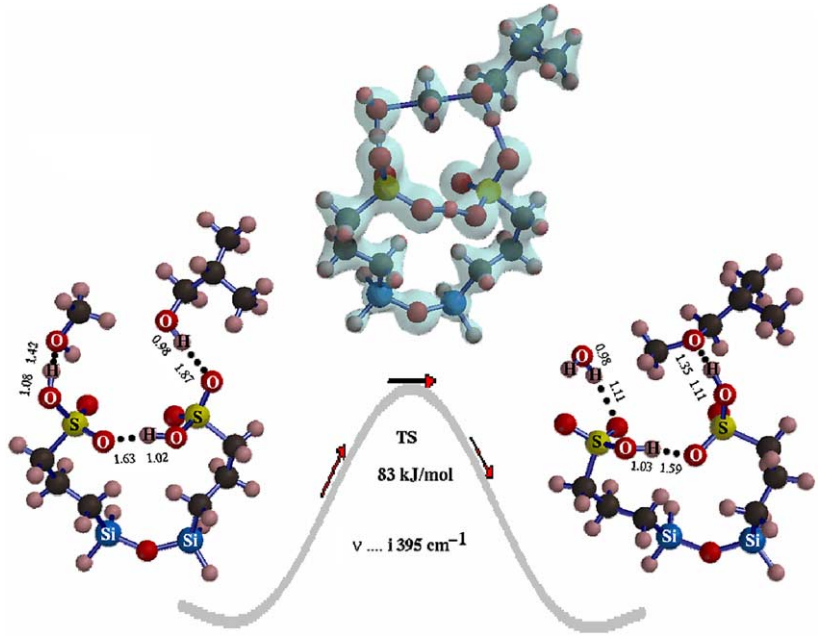

Fig. 8. The optimized configuration, left, of adsorbed MeOH and i-BuOH molecules on the proximal sulfonic acid centers on the SBA-15 catalyst. The transition state for the reaction of MeOH with i-BuOH to form MIBE over SBA-15 is shown in the middle, where electron density is shown as a transparent isosurface to within 0.08 electrons/a.u.^{3} The optimized configuration of adsorbed MIBE and H_2O product molecules on proximal sulfonic acid centers of the SBA-15 catalyst is shown on the right. Selected distances of importance to the adsorption and reaction are given in Å.

The TS for the reaction pathway is shown in Fig. 7, middle. The electron density isosurface in the TS, within 0.08 electrons/a.u.^{3}, clearly indicates the bonds of the transferred methyl group with the O atoms of the two alcohols being symmetrically severed while the methyl group assumes a planar structure. The formed ether and water molecules leave the active sites as the transfers of two protons to different oxygens in the sulfonic groups are completed, as shown in Fig. 7, right.

The path to MIBE is similar to that depicted for DME. The adsorption configuration of MeOH and i-BuOH on the sulfonic acid centers to form the G=$(OH)_2$(MeOH)(i-BuOH) complex is shown in Fig. 8, left, with pertinent H-bond distances designated. The optimized TS for MIBE

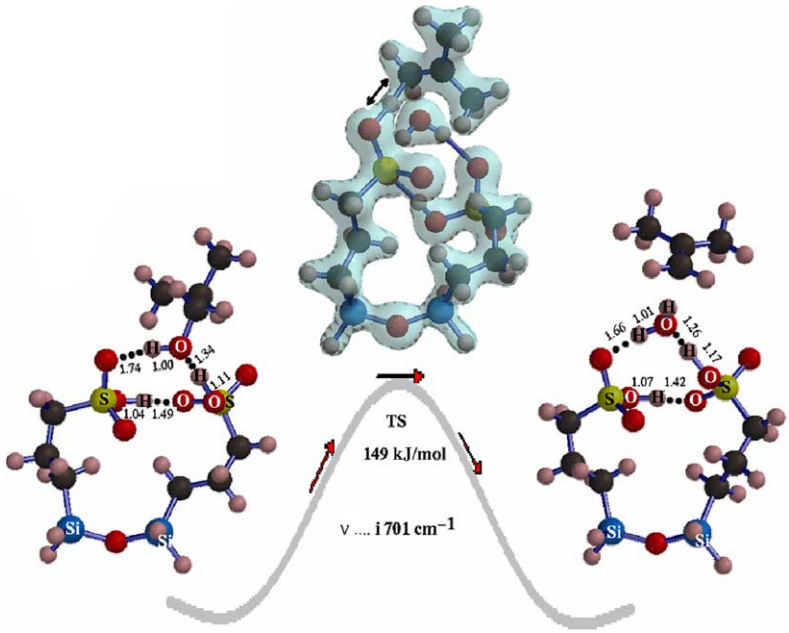

Fig. 9. The optimized configuration, left, of an adsorbed i-BuOH molecule on a sulfonic acid center on the SBA-15 catalyst, also showing interaction with an adjacent unoccupied sulfonic acid group. The transition state for isobutanol dehydration over SBA-15 is shown in the middle of the figure, where electron density is shown as a transparent isosurface to within 0.08 electrons/a.u.[3] The optimized configuration of the products of dehydration of isobutanol is shown on the right. Selected distances of importance to the adsorption and dehydration are given in Å.

Table 5
The calculated adsorption energies of reactants, products, and poisons onto single-site $–SO_3H$ with an adjacent noninteracting –SH group on the SBA-15 surface modeled as $HS(CH_2)_3–Si(H)_2–O–Si(H)_2–(CH_2)_3\mathbf{SO_3H}$

Adsorbate	Single-site adsorption energy (kJ/mol)	Dual-site adsorption energy (kJ/mol)
i-BuOH	−54.5	−50.7
MeOH	−46.5	−44.8
MIBE	−29.9	−8.5
H_2O	−22.2	−17.6
DME	−26.5	−8.9
IB	−7.4	+33.3
Py	−55.3	−34.3
NH_3	−74.6	−79.7
En[a]	−96.1	−83.6

Comparison is made with the adsorption energies calculated with a dual reactive site modeled as $\mathbf{HO_3S}(CH_2)_3–Si(H)_2–O–Si(H)_2–(CH_2)_3\mathbf{SO_3H}$. To simulate the rigidity of the silica wall, the seven atoms of the –Si–O–Si– backbone capped by four hydrogen atoms were kept frozen in all geometry optimizations in which all other atoms were allowed to move.
[a] En, ethylenediamine.

formation is shown in Fig. 8, middle. Subsequently, the MIBE and H_2O products form the weakly bonded postreaction complex, Fig. 8, right.

The stationary points of the path (**V**) → (**VI**) for dehydration of i-BuOH to IB are shown in Fig. 9. Fig. 9, left, depicts adsorbed i-BuOH and Fig. 9, middle, shows TS $G{=}(OH)_2(i\text{-}Bu^{=})(H_2O)$. The main motion of the TS imaginary mode is indicated by the double-ended arrow, between the C-1 carbon of i-BuOH and an oxygen of one sulfonic group, while the water is already dissociated and "parked" on the second sulfonic group of the dual site. The product side in Fig. 9, right, reveals weakly hydrogen-bonded water and "flown away" isobutene that is no longer bonded to any of the two sites.

The energies of adsorbed reactant couples, product molecules, and water given above are consistent with those of the individual adsorbed molecules, each on a single-site $–SO_3H$ on the SBA model surface. The calculated adsorption energies are given in Table 5, with the addition of sorption energies of nitrogen bases that act as catalytic poisons for the reaction studied herein. Modeling of adsorption onto dual interacting surface sites follows the same trend in adsorption energies.

4. Discussion

4.1. Ethers from alcohols

4.1.1. Ether synthesis from MeOH/i-BuOH = 1/1 reactants

As the reaction pressure was increased at 404 K with a constant flow rate of the MeOH/i-BuOH = 1/1 reactant mixture, the formation rates of the ethers steadily increased (Fig. 2). In contrast, the rate of dehydration of isobutanol to form isobutene, as well as the 2-butenes, increased sharply as the pressure was initially increased and then gradually declined with higher pressure to yield a broad maximum. The data points in Fig. 2 were fitted with solid lines by using the kinetic laws represented by Eqs. (1)–(3) (Section 2.3). This yielded the values of $K_M = 0.015\ \mathrm{kPa}^{-1}$, $K_B = 0.040\ \mathrm{kPa}^{-1}$, $K_1 = 1.47\ \mathrm{mol/(kg_{cat}\,h)}$,

$K_3 = 0.801$ mol/(kg_{cat} h), and $K_4 = 1.62$ mol/(kg_{cat} h). The larger adsorption equilibrium constant for i-BuOH relative to that for MeOH ($K_B/K_M = 2.67$) indicates that i-BuOH is more strongly held by the acid sites than the MeOH reactant and is consistent with the relative basicity of the two alcohols and the observations obtained with other catalysts [17,26,36,46,51]. This is also consistent with the calculated adsorption energies of the reactants (Table 5). The rate of IB formation passes through a maximum, consistent with Eq. (3).

At ambient pressure (101.3 kPa), the steady-state synthesis rate of all products increased as the reaction temperature was increased, and in particular the dehydration of isobutanol to form isobutene was greatly favored. This was accompanied by decreasing selectivities toward the formation of all of the ethers, especially MIBE. The apparent activation energies (E_a), shown in Fig. 3, demonstrated that the E_a values for isobutene and the 2-butenes (150–160 kJ/mol range) were *appreciably* higher than those for the ethers, with DME at 113 kJ/mol, MIBE and DIBE in the 75–80 kJ/mol range, and MTBE and TBIBE in the 40–60 kJ/mol range under these reaction conditions. This is also consistent with the high TS barrier calculated for the dehydration of i-BuOH to form IB (Table 3). Clearly, low temperatures favored ether synthesis.

4.1.2. Ether synthesis from MeOH/i-BuOH = 2/1 reactants

Increasing the MeOH/i-BuOH ratio to 2/1 at 404 K significantly decreased the rate of dehydration of i-BuOH to IB while enhancing the dehydrocondensation reactions to form MIBE and DME, as shown in Fig. 4. MIBE was the dominant product formed, and only traces of MTBE, DIBE, and 2-butenes were observed. The solid lines in Fig. 4 were obtained by using the kinetic laws represented by Eqs. (1)–(3) and maintaining the same values of K_M and K_B as determined with the MeOH/i-BuOH = 1/1 reaction test. This resulted in the values of $K_M = 0.015$ kPa^{-1}, $K_B = 0.040$ kPa^{-1}, $K_1 = 1.13$ mol/(kg_{cat} h), $K_3 = 0.474$ mol/(kg_{cat} h), and $K_4 = 1.51$ mol/(kg_{cat} h) being obtained for this MeOH/i-BuOH = 2/1 experiment. Again, the kinetic rate constant for the MIBE synthesis reaction, K_4, exhibited the largest value.

The experimental data in Fig. 4 at an isobutanol partial pressure of 100 kPa (300 kPa total alcohol pressure; 3.27 MPa total pressure) correspond to the rate of formation of MIBE of about 25 g/(kg_{cat} h) at 404 K with a selectivity of 60%. At approximately these same reaction conditions with MeOH/i-BuOH = 2/1, but at 389 K, a Nafion-H microsaddles catalyst exhibited a productivity of 27 g MIBE/(kg_{cat} h) with a selectivity of 66% [16,17]. With the present SBA-15 catalyst, the selectivity to MIBE remained almost constant at about 60% at elevated reaction pressures, and this selectivity behavior is similar to that observed with the Nafion-H microsaddles catalyst [16,17].

While maintaining a 2.17 MPa reaction pressure over the SBA-15 catalyst, increasing reaction temperature with a MeOH/i-BuOH/N_2 = 10.4/5.2/184 mol/(kg_{cat} h) reactant stream resulted in increased rate of formation of all three products. Again, higher temperatures promoted the formation of IB to a larger degree than the ethers. In this case, the DME selectivity decreased only slightly (from 29.5 to 25.4% in the temperature range studied), while the MIBE selectivity decreased from 70.5 to 46.7% as the IB selectivity increased from zero to 27.9%. The greater enhancement of the rate of formation of IB with increasing temperature is again reflected in the higher E_a value of IB relative to the ethers, 218 kJ/mol for IB compared with 102 and 89 kJ/mol for DME and MIBE, respectively (Fig. 5). These apparent activation energies are in the same order as those observed with a Nafion-H microsaddles catalyst, with data obtained from Fig. 6 of Ref. [17], for product formation in the 389–430 K temperature range from a MeOH/i-BuOH/N_2 = 10.4/5.2/186 mol/(kg_{cat} h) reactant stream at 7.58 MPa, i.e., for IB, DME, and MIBE the E_a values were 222, 75, and 68 kJ/mol, respectively. In all cases with the different catalysts, the MIBE product exhibited the lowest apparent activation energy. If isobutene were the desired product, high i-BuOH/MeOH ratios and low reaction pressure, along with higher temperatures, should be utilized.

4.2. Deactivation of the SBA-15 catalyst by pyridine

The catalyst was stable during testing, as demonstrated in Table 1. To probe blocking of the active Brønsted acid sites, exposure of the catalyst to pyridine was carried out at 404 K and 375 kPa. As the Py reached the catalyst, the rates of formation of all products decreased, as indicated in Fig. 6. The decrease was initially most evident by loss of IB formation, while at the time no Py was detectable in the exit gas stream. This indicates that the Py was adsorbing onto the catalyst, particularly the unoccupied sulfonic sites first, which are acceptor sites for water during the E2 dehydration of isobutanol [51], resulting in a delay in Py breakthrough in the exit gas. Further exposure of the catalyst to Py led to complete inhibition of the coupling reactions.

Purging the catalyst with N_2 at the reaction temperature and pressure did not regenerate the catalyst. However, increasing the temperature or pressure did yield the expected products, but in much smaller yields than observed before the Py exposure (Table 2). In particular, the synthesis of IB was retarded. After the 473 K test, lowering the temperature to the original reaction condition did not lead to regeneration of the catalytic activity. Thus, the higher temperature did not regenerate the acid sites that were previously active at the lower temperatures. This is due to pyridine retention revealed by N1s XPS analysis as described below.

4.3. Analysis of the SBA-15 catalyst

The initial SBA-15 material was completely devoid of residues of the Pluronic surfactant, and the C/S ratio of 2.9 is near the stoichiometry of $-(CH_2)_3SO_3H$ [37]. All the S was oxidized, and none was detectable as thiol groups. When Py was adsorbed, the S2p core-level shift (CLS) was in the direction of lower BE, while the N1s of Py shifted to higher BE (402.2 eV vs 400.3 eV for solid Py [52]). Details of such acid–base interactions and corresponding CLS calculations are given in our preceding paper [37]. In the present study, the S2p BE peak was resolved into two peaks, S(1) = 169.1 eV and S(2) = 167.8 eV, with S(1) having nearly the same BE as the S2p in SBA-15 prior to pyridine adsorption (169.25 eV [37]). Quantitative resolution of the S2p spectrum into two S2p peaks for the tested sample gave a S(2)/(S(1) + S(2)) ratio = 0.28, which is the same ratio as observed for the $N/S_{(Total)}$ equivalence (Section 3.5). Therefore, the Py is coordinated to S(2), and the S(2) S2p CLS of 1.3–1.45 eV to *lower* BE corresponds to the N1s CLS to *higher* BE by approximately 2 eV. These CLSs are consistent with direct interaction of the Py via its nitrogen with a Brønsted acid functionality associated with the sulfonic $-SO_3H$ group, i.e., $\equiv Si-(CH_2)_3SO_3\cdots H\cdots NC_5H_5$ whereby the proton donor group $-SO_3H$ undergoes CLS in the opposite direction to that of the coordinating nitrogen base [37,46,48].

Prolonged catalytic testing and partial Py poisoning of the SBA-15 catalyst resulted in excess carbon on the catalyst and BET surface area of 314 m^2/g. The mesopore structure of the material was maintained, as shown by a narrow pore-size distribution and by TEM micrographs of the tested catalyst showing long-range order of the one-dimensional tubular channels in the particles. Measurements yield a pore center-to-center distance (a) of 11.0 ± 0.2 nm, with the pore mouth diameters of 7.0–7.5 nm. Using the diameter of the mesopores determined by N_2 adsorption ($d_p = 7.7$ nm) and the total pore volume ($V_p = 0.60\ cm^3/g$) determined from the adsorption isotherm, the specific surface area of mesopore structures was calculated by using the geometric relationship $S_{meso} = (4V_p)/d_p$ [53] to be 312 m^2/g. This is in agreement with the BET surface area of the tested catalyst, indicating no contribution to the surface area and total pore volume by micropores. After Py poisoning, carbon residue probably blocked pores and access to active sites.

4.4. Theory of reactant bonding, prereaction complexes, stationary points on the three principal reaction pathway, and reaction mechanisms

The present theory not only yields adsorption and reaction patterns that are fully consistent with mechanisms based on earlier isotope studies, product composition, and the current experimental observations, but also affords predictions regarding catalyst design. We address the specific features as listed below.

4.4.1. Single adsorbates and multiple adsorbates

All the oxygen-containing species, alcohols, ethers, and water, are bonded to the sulfonic groups O-down by an acceptor hydrogen bond following the order of bonding strengths, i-BuOH > MeOH > MIBE > water > DME (single site model in Table 5). Isobutene is very weakly bonded (−7.4 kJ/mol) and this molecule is completely displaced when other oxygen-containing molecules, including the weakly bonded ethers and water (−30 to −13 kJ/mol), are competing for the reaction site. Nitrogen bases are strongly bonded, as expected. Of those, pyridine is the weakest base but still is bonded more strongly than the oxygenated reactants and products. In all cases, the proton of the sulfonic acid group is not transferred to the oxygen or nitrogen of the adsorbate – only H bonding of varying strengths is involved here, in contrast to the perfluoro-alkylsulfonic acids that do transfer their protons to pyridine to form pyridinium [37,48].

When two proximal sites are occupied by reactants or products, interactions result in changes of configurations that include donor hydrogen bonding of an –OH group of alcohol or water to an O=S group of the sulfonic acid site. This is exemplified by the bonding of two methanol molecules to the proximal sites in Fig. 7. Here the S–OH group of one sulfonic group acts as a "normal acid site" for one methanol while the O=S group of the second sulfonic group acts as a basic site for the second methanol molecule. This situation repeats itself in simultaneous bonding of methanol and isobutanol as in Fig. 8, and even with water hydrogen-down in the products of dehydrocondensations in Figs. 7 and 8. *In general terms, the acid functionality of one sulfonic site, when utilized as a hydrogen-donor site, changes the proximal site's function to one of a hydrogen-bond acceptor*. In the dual-site model, interaction via hydrogen bonding lowers the adsorption energies of the products (Table 5), favoring their desorption from the catalyst surface compared to the single sites. In the case of the dual-site adsorption of the reactants in particular, the H bonding between the neighboring sites is not only an energy-determining feature but a structure-determining feature as well. This is evident from stretched S–O···H and shortened S–OH···O=S distances in all dual-site models in Figs. 7–9.

4.4.2. Reaction pathways

In all reactions studied, the overall TS barrier height and its connectivity with reactants and products are strongly influenced by the concerted motion of the "far away" atoms and flexibility of the entire dual-site ensemble with the H-bonded reactants. This is in complete agreement with conclusions drawn from simpler models for this class of reactions [54].

In the dehydrocondensation of alcohols to ethers, the results show convincingly that dissociation–reassociation of the C–O bond in the adsorbed methanol subject to "rear attack" onto its inverting methyl group is the dominant feature of the reaction pathway at the TS. In the TS complex, motions of all atoms associated with the TS imaginary modes

occur, in particular the "umbrella inversion" of the CH_3 group in opposite phases of their vibrations, passing through a planar "sp^2" configuration as it is inverted upon moving from the MeOH molecule to the oxygen end of the second alcohol to form DME (Fig. 7) or MIBE (Fig. 8). At the same time, there is a cyclic transfer of three H atoms among the sulfonic acid groups and the two reacting alcohols that results in the release of water molecules formed from the oxygen originally in the MeOH molecules, consistent with selective rejection of ^{18}O from Me ^{18}OH in earlier observed MIBE synthesis [22–24]: the proton from the first sulfonic acid site attacks methanol, its methyl group is being transferred to the second alcohol whose proton is moving toward the base O=S of the second sulfonic group, and its proton is moving to the first sulfonic group to render it electrically neutral. Examination of computed charges indicates that this *proton transfer between neighboring sites minimizes charge imbalance in the TS*. The theoretical barriers for the DME and the MIBE reactions are quite close (73 and 83 kJ/mol, respectively, Table 3), although their relative values are opposite to experimental apparent activation energies (see Figs. 3 and 5). These calculated barriers are, however, remarkably close to the experimental activation energies. The imaginary vibrational modes of the TS have nearly identical frequencies, within one wavenumber of 394 cm^{-1} (Table 4).

The mechanism for dehydration of isobutanol to isobutene and the associated reaction parameters are quite different: the E2 mechanism, previously proposed for this reaction based on kinetics [51], is operating here too, with the following features: the prereaction complex is i-BuOH bonded O-down on one hydrogen-donor site (I), but also H-down to the other acceptor site (II) (Fig. 9, left); then proton of site I attacks the OH group of the alcohol and water leaves to be "parked" on site I. The TS involves abstraction of H originally bonded to C-2 which, however, has already traveled to C-1. Its 700 cm^{-1} imaginary mode (Table 4) is indicated by an arrow in Fig. 9, middle. The acceptor of this proton is the basic O=S group of site II. The frequency of this mode that is associated with proton transfer is substantially higher than those associated with methyl transfer in the DME- and MIBE-forming reactions. The postreaction complex is water-bonded O-down to the proton of site I with the unbonded, planar isobutene released away. The theoretical barrier of 149 kJ/mol is much higher than that for the DME and MIBE reactions (Table 3), is comparable to the experimental apparent activation energy determined at ambient pressure (161 kJ/mol, Fig. 3), but is lower than the 218 kJ/mol obtained at higher pressures, under which the ether synthesis dominates the prereaction adsorption equilibria and blocks the sites for water release in isobutanol dehydration.

4.4.3. Poisoning by pyridine

The theoretical adsorption energy of pyridine on a single acid site, −55.3 kJ/mol, is comparable to that of isobutanol and substantially larger than that of any other reactant or product (Table 5). This has the consequence not only of blocking the sulfonic acid sites for adsorption and activation of methanol, the reactant for the ether formation, but also of blocking the sites for water in the E2 dehydration of isobutanol. This is in agreement with experimental observation (Fig. 6).

4.4.4. Relation to kinetics

Even though the present model is idealized, it successfully confirms the dual-site S_N2 mechanism as the most efficient pathway for ethers and the E2 mechanism for dehydration of isobutanol. The dual-site mechanism is consistent with kinetics in that increased pressure increases the DME and MIBE formation in a parallel fashion, but strongly suppresses the E2 reaction by adsorbed alcohols blocking the acceptor sites for water. The model holds generally, and the kinetic patterns are very similar for several classes of solid acids–polymeric, derivatized inorganic oxides [16–24,26,36,46,51,54] and now the SBA material.

4.4.5. Some theoretical predictions for catalyst design

Apart from the generality of the reaction mechanism and the advantage of large-pore spaces in the SBA material that allows extension of the present reaction types to large molecules, some theoretical predictions for catalyst design can be made: (1) because of the cyclic proton shuttling among the proximal catalyst sites accompanying the S_N2 alkyl transfer, the most efficient catalysts for dehydrocondensation of alcohols to ethers will require large surface concentrations of the acid sites, ideally one propylsulfonic group tethered to each surface Si atom; (2) dehydration of the higher alcohol can be promoted by low pressures that provide for empty acceptor sites for water, and will be suppressed at high pressures for the opposite reason—however, the proton capture from the TS will be facilitated by a stronger base than the present O=S group; and (3) partial or total fluorination of the alkylsulfonic groups will increase the acid strength, or proton-donating ability, of one site, and cation exchange of protons on the neighboring site will increase its proton-accepting ability. The background for testing the theory has been developed; in particular XPS core-level shifts were found a useful probe for the theoretically predicted effects of weakly and strongly hydrogen-bonded adsorbates [37].

5. Conclusions

SBA-15 is a stable mesoporous silica-based catalyst for synthesis of ethers from alcohols. The propylsulfonic acid groups anchored on the pore walls are robust and maintain their Brønsted acid functionality even after prolonged testing. However, these hydrocarbon sulfonic sites, even though weaker acids than fluorocarbon sulfonic groups, are easily poisoned by the presence of the nitrogen base pyridine in the reactant mixture. Full regeneration of the activity of the

catalyst after deliberate poisoning was not successful under the mild reaction conditions utilized.

There is no direct pathway for MTBE formation from MeOH and i-BuOH reactants. The dominant reaction pathways are: (1) ether synthesis by S_N2 rear attack of one alcohol on a second alcohol molecule to yield MIBE and DME, and (2) dehydration of i-BuOH to yield IB via a carbenium-type intermediate in an E2-type pathway. Isobutene is only weakly adsorbed on the active sites of SBA-15; thus, little of this product reacts with MeOH to form MTBE via an indirect pathway before desorbing. Very small amounts of side-product *n*-butenes, DIBE, and TBIBE were observed and are deemed insignificant for the kinetic and quantum mechanical modeling of the main pathways.

Selectivity for the products formed from the alcohols can be controlled by the following reaction conditions:

1. At lower reaction pressures, i-BuOH is preferentially adsorbed from MeOH/i-BuOH reactant mixtures on sulfonic acid groups, and with adjacent unoccupied sites, the initial dominant product is IB;
2. As the reaction pressure increased, adsorption of MeOH increased, and the productivity of the ethers increased at the expense of IB;
3. At lower reaction temperatures, ethers were the dominant products formed, consistent with the lower experimental apparent activation energies and calculated TS barriers along the reaction coordinate; and
4. As the reaction temperature increased, the product selectivity shifted toward IB, consistent with its high apparent activation energy and TS barrier.

For optimum synthesis of ethers, low reaction temperature and elevated pressures should be utilized with catalysts having a high concentration of Brønsted acid sites in close proximity to one another.

Acknowledgments

We acknowledge the support of this work by the US Department of Energy (DE-FG02-01ER15181). We thank Dr. Alfred C. Miller for professional and technical assistance with the XPS analyses using the Scienta ESCA facility of Lehigh University.

References

[1] Kirk–Othmer Encyclopedia of Chemical Technology, vol. 11, third ed., Wiley, New York, 1980, pp. 410–425.
[2] D.E. Ridler, M.V. Twigg, in: M.V. Twigg (Ed.), Catalyst Handbook, second ed., Wolfe, London, 1989, p. 225.
[3] J.R. LeBlanc, R.V. Schneider III, R.B. Strait, in: W.-H. Cheng, H.H. Kung (Eds.), Methanol Production and Use, Dekker, New York, 1994, p. 51.
[4] G.W. Bridger, M.S. Spencer, in: M.V. Twigg (Ed.), Catalyst Handbook, second ed., Wolfe, London, 1989, p. 441.
[5] S. Lee, Methanol Synthesis Technology, CRC Press, Boca Raton, FL, 1990.
[6] C.D. Chang, Hydrocarbons from Methanol, Dekker, New York, 1983.
[7] R.G. Herman (Ed.), Catalytic Conversions of Synthesis Gas and Alcohols to Chemicals, Plenum, New York, 1984.
[8] H. Papp, M. Baerns, Stud. Surf. Sci.Catal 64 (1991) 430.
[9] H.H. Kung, K.J. Smith, in: W.-H. Cheng, H.H. Kung (Eds.), Methanol Production and Use, Dekker, New York, 1994, p. 175.
[10] C.D. Chang, in: W.-H. Cheng, H.H. Kung (Eds.), Methanol Production and Use, Dekker, New York, 1994, p. 133.
[11] K. Smith, R.B. Anderson, Can. J. Chem. Eng. 61 (1983) 40.
[12] G.A. Vedage, P. Himelfarb, G.W. Simmons, K. Klier, Prepr. Am. Chem. Soc., Div. Pet. Chem. 28 (1983) 1261.
[13] J.G. Nunan, C.E. Bogdan, K. Klier, K.J. Smith, C.-W. Young, R.G. Herman, J. Catal. 116 (1989) 195.
[14] J.G. Nunan, R.G. Herman, K. Klier, J. Catal. 116 (1989) 222.
[15] A. Beretta, Q. Sun, R.G. Herman, K. Klier, Ind. Eng. Chem. Res. 35 (1996) 1534.
[16] J. Nunan, K. Klier, R.G. Herman, J. Chem. Soc., Chem. Commun. (1985) 676.
[17] J.G. Nunan, K. Klier, R.G. Herman, J. Catal. 139 (1993) 406.
[18] R.G. Herman, K. Klier, O.C. Feeley, M.A. Johansson, Prepr. Am. Chem. Soc., Div. Fuel Chem. 39 (1994) 343.
[19] K. Klier, R.G. Herman, M.A. Johansson, O.C. Feeley, Prepr. Am. Chem. Soc., Div. Fuel Chem. 37 (1992) 236.
[20] R.G. Herman, K. Klier, O.C. Feeley, M.A. Johansson, Q. Sun, L. Lietti, Prepr. Am. Chem. Soc., Div. Fuel Chem. 39 (1994) 1141.
[21] O.C. Feeley, M.A. Johansson, R.G. Herman, K. Klier, Prepr. Am. Chem. Soc., Div. Fuel Chem. 37 (1992) 1817.
[22] Q. Sun, R.G. Herman, K. Klier, J. Chem. Soc., Chem. Commun. (1995) 1849.
[23] O.C. Feeley, Q. Sun. R.G. Herman, M. Johansson, L. Lietti, K. Klier, Catal. Lett. 35 (1995) 13.
[24] K. Klier, Q. Sun, O.C. Feeley, M. Johansson, R.G. Herman, Stud. Surf. Sci. Catal 101 (1996) 601.
[25] J.G.C. Shen, T.H. Kalantar, R.G. Herman, J.E. Roberts, K. Klier, Chem. Mater. 13 (2001) 4479.
[26] J.G.C. Shen, T.H. Kalantar, Q. Ma, R.G. Herman, K. Klier, J. Chem. Soc., Chem.Commun. (2001) 653.
[27] C.T. Kresge, M.E. Leonowicz, W.J. Roth, J.C. Vartuli, J.S. Beck, Nature 359 (1992) 710.
[28] J.S. Beck, J.C. Vartuli, W.J. Roth, M.E. Leonowicz, C.T. Kresge, K.D. Schmitt, C.T.-W. Chu, D.H. Olson, E.W. Sheppard, S.B. McCullen, J.B. Higgins, J.L. Schlenker, J. Am. Chem. Soc. 114 (1992) 10834.
[29] D. Zhao, J. Feng, Q. Huo, N. Melosh, G.H. Fredrickson, B.F. Chmelka, G.D. Stucky, Science 279 (1998) 548.
[30] D. Zhao, Q. Huo, J. Feng, B.F. Chmelka, G.D. Stucky, J. Am. Chem. Soc. 120 (1998) 6024.
[31] D. Margolese, J.A. Melero, S.C. Christiansen, B.F. Chmekla, G.D. Stucky, Chem. Mater. 12 (2000) 2448.
[32] W.M. Van Rhijn, D.E. De Vos, B.F. Sels, W.D. Bossaert, P.A. Jacobs, J. Chem. Soc., Chem. Commun. (1998) 317.
[33] M.H. Lim, C.F. Blanford, A. Stein, Chem. Mater. 10 (1998) 467.
[34] W.D. Bossaert, D.E. De Vos, W.M. Van Rhijn, J. Bullen, P.J. Grobet, P.A. Jacobs, J. Catal. 182 (1999) 156.
[35] I. Díaz, F. Mohino, J. Pérez-Pariente, E. Sastre, Appl. Catal. A 205 (2001) 19.
[36] J.G.C. Shen, R.G. Herman, K. Klier, J. Phys. Chem. B 106 (2002) 9975.
[37] J.L. Smith, R.G. Herman, C.R. Terenna, M.R. Galler, K. Klier, J. Phys. Chem. A 108 (2004) 39.
[38] I.K. Mbaraka, D.R. Radu, V.S.-Y. Lin, B.H. Shanks, J. Catal. 219 (2003) 329.
[39] R.A. Hunsicker, K. Klier, T.S. Gaffney, J.G. Kirner, Chem. Mater. 14 (2002) 4807.
[40] S. Brunauer, P.H. Emmet, E. Teller, J. Am. Chem. Soc. 60 (1938) 309.

[41] E.P. Barrett, L.G. Joyner, P.P. Halenda, J. Am. Chem. Soc. 73 (1951) 373.
[42] S.J. Gregg, K.S.W. Sing, Adsorption, in: Surface Area, and Porosity, Academic Press, London, 1967, pp. 160–172.
[43] M. Kruk, M. Jaroniec, C.H. Ko, R. Ryoo, Chem. Mater. 12 (2000) 1961.
[44] Y. Wang, M. Noguchi, Y. Takahashi, Y. Ohtsuka, Catal. Today 68 (2001) 3.
[45] W.-H. Zhang, J. Lu, B. Han, M. Li, J. Xiu, P. Ying, C. Li, Chem. Mater. 14 (2002) 3413.
[46] K. Klier, H.-H. Kwon, R.G. Herman, R.A. Hunsicker, Q. Ma, S.J. Bollinger, Stud. Surf. Sci. Catal. 130D (2000) 3447.
[47] Specific functionals are: A.D. Becke, Phys. Rev. A 38 (1988) 3098; J.P. Perdew, A. Zunger, Phys. Rev. B 23 (1981) 5048; J.P. Perdew, Phys. Rev. B 33 (1986) 8822, Phys. Rev. B 34 (1986) 7406 (erratum).
[48] M. Johansson, K. Klier, Top. Catal. 4 (1997) 99.
[49] J.F. Moulder, W.F. Stickle, P.E. Sobul, K.D. Bomben, in: J. Chastain (Ed.), Handbook of X-Ray Photoelectron Spectroscopy, Perkin–Elmer Corp., Eden Prairie, MN, 1992.
[50] G. Beamson, D. Briggs, High Resolution XPS of Organic Polymers: The Scienta ESCA300 Database, Wiley, Chichester, 1992.
[51] L. Lietti, Q. Sun, R.G. Herman, K. Klier, Catal. Today 27 (1996) 151.
[52] S. Suzuki, Y. Yamaguchi, H. Onishi, T. Sasaki, K. Jukui, Y. Iwasawa, J. Chem. Soc., Faraday Trans. 94 (1998) 161.
[53] M. Kruk, M. Jaroniec, A. Sayari, Langmuir 13 (1997) 6267.
[54] K. Klier, Top. Catal. 18 (2002) 141.